1 **Variable patterns of phenotypic evolution among canonical 'living fossil' lineages**

2 Rafael A. Rivero-Vega[1*], Jacob S. Berv[1,2], John T. Clarke[3-8], & Matt Friedman[1]

3 Coelacanths, lungfishes, and holosteans represent three emblematic living fossil lineages,
4 thought to be united by similar patterns of phenotypic change through time. While past studies
5 suggest that diverse evolutionary patterns occur within these groups, it is unclear whether these
6 reflect biological differences or arise from contrasting analytical approaches. Here, we examine
7 these lineages under a common framework to assess variation in the evolution of discrete
8 characters, and morphometric shape data, to test whether living fossils show comparable patterns
9 of phenotypic evolution. Our results suggest different evolutionary modes occur, both among and
10 within lineages, as a function of data type. For lungfishes, rates in discrete characters are highest
11 in the Devonian and monotonically decline over time. Coelacanth rates show multiple early
12 peaks followed by a decline toward the recent. Holostean rates show modest peaks but are
13 broadly comparable over time. Patterns of body shape evolution also differ among clades, with
14 strong support for declining rates over time for coelacanths but mixed evidence for similar
15 dynamics in the other groups. Our results imply idiosyncratic processes of evolutionary change
16 among traditional examples of living fossils and indicate a need to explicitly quantify patterns of
17 change rather than apply informal, often qualitative, macroevolutionary classifications.
18

19 Corresponding Author: *Rafael A. Rivero-Vega[1], rarivero@umich.edu
20
21 *1. Museum of Paleontology and Department of Earth and Environmental Sciences, University of*
22 *Michigan, Ann Arbor, Michigan, 48108-1079, U.S.A.*
23
24 *2. Department of Ecology and Evolutionary Biology, University of Michigan, Ann Arbor,*
25 *Michigan, 48108-1079, U.S.A.*
26
27 *3. German Centre for Integrative Biodiversity Research (iDiv) Halle- Jena- Leipzig, Leipzig,*
28 *Germany. E-mail: j.clarke.paleo@gmail.com*
29
30 *4. Institute of Biodiversity, Friedrich Schiller University Jena, Jena, Germany*
31
32 *5. GeoBio-Center, Ludwig-Maximilians-Universität München, Richard-Wagner-Str. 10, 80333*
33 *Munich, Germany*
34
35 *6. Department of Earth and Environmental Sciences, Paleontology & Geobiology, Ludwig-*
36 *Maximilians-Universität München, Richard-Wagner-Str. 10, 80333 Munich, Germany*
37
38 *7. Department of Ecology and Biogeography, Nicolaus Copernicus University in Toruń,*
39 *Lwowska 1, 87-100, Toruń, Poland*

40

41   *8. Department of Zoology, Institute of Ecology and Earth Sciences, University of Tartu, Liivi 2,*

42   *50409 Tartu, Estonia*

43

1. Introduction

44

45   "Living fossil"—a term coined by Darwin [1]—is one of the most evocative ideas in evolutionary

46   biology. Like many concepts first articulated in *On the Origin of Species*, the initial account of

47   living fossils combined careful natural history observations with hypotheses of their origins.

48   Darwin provided three examples of living fossils: ganoid fishes (bichirs, sturgeons, paddlefishes,

49   gars, and the bowfin), *Ornithorynchus* (platypus), and *Lepidosiren* (South American lungfish) ([1]:

50   p. 107). These groups were, Darwin argued, united by a set of common features. First, each

51   contained the last survivors of lineages that the fossil record indicates were once much more

52   diverse. Second, all three represented structural intermediates between more species-rich groups

53   (chondrichthyans and teleosts in the case of 'ganoids', reptiles and mammals in the case of

54   *Ornithorhynchus*, and fishes and tetrapods in the case of *Lepidosiren*). Third, all are restricted to

55   specific, often spatially limited habitats. Darwin saw in this final observation a potential

56   explanation for the first two features of living fossils: endurance of such lineages might reflect

57   reduced competition encountered in geographically or environmentally restricted settings.

58   Since Darwin's proposal, the concept of living fossils has been widely applied across the tree of

59   life [2]. As the set of lineages interpreted as living fossils has expanded, the concept's meaning has

60   grown so diffuse that its utility is hotly debated [3–9]. Investigations into the dynamics of

61   phenotypic evolution reflect a shift from Darwin's original formulation of living fossils to more

62   recent conceptualisations [10,11]. Although Darwin only indirectly addressed processes of

63   morphological change in these groups, aspects of evolutionary tempo and mode responsible for

64   patterns of phenotypic variation are central to many of today's applications of the living fossil

65   concept (e.g., see criteria in [7]). Generally, the phenotypic variation in living fossil groups is

66   interpreted as either uniformly low [12], subject to strong evolutionary constraint [13], or declining

67   over time [14,15], with the latter being more prevalent in the recent literature (e.g., *Sphenodon*

68   [15]). With some exceptions [16], quantitative investigations of phenotypic evolution in putative

69   living fossil lineages are restricted to isolated examples. While some aspects of tempo and mode

70   may be shared, assessing these lineages independently prevents fair comparisons among them

71   [14,17–21].

72   To assess the degree of macroevolutionary convergence in aspects of phenotypic evolution among

73   the most prominent examples of living fossils, we combined existing and newly collected

74   morphological data and analysed each taxon in a consistent framework. Our goal is not to test *a*

75   *priori* expectations of specific macroevolutionary patterns. Instead, we look to test whether our

76   canonical living fossil groups share comparable patterns of phenotypic change over time. Such

77   similarity is implied by much of the recent literature on living fossils [14,15]; however, it is not

78   reflected in Darwin's three defining characteristics of such groups. In essence, we are testing

79   whether the gross patterns that unite living fossils might be generated by similar underlying

80   histories of evolutionary change. This approach is similar to that of "phylogenetic natural history"

81   *sensu* Uyeda et al. 2018 [22], with the aim of documenting phylogenetic evidence of evolutionary

82   process. Importantly, we do not seek a numerical measure of potential "living fossil"-ness like

83   some recent work [23]. Rather, our methodological approach is inspired by recent cross-clade

84   comparative approaches used to evaluate adaptive radiations [24,25], another macroevolutionary

85   concept that had come to be broadly—and at times imprecisely—applied since it was first

86   articulated [24,26–30]. We take a restricted approach, emphasising two of the lineages first

87   identified by Darwin: lungfishes and holosteans. Darwin's third example, monotremes, are too

88   scarce in the fossil record [31] to offer a helpful comparison, so we examine coelacanths instead.

89   Though obviously not considered by Darwin because eight decades separate the publication of

90   *Origin* from the naming of the living *Latimeria*, coelacanths conform to the original definition of

91   living fossils. Features common to these three groups make them ideal for the comparative study

92   of phenotypic evolution: a long history of systematic and paleontological examination, established

93   phylogenetic frameworks, and articulated fossils that provide perspectives on changes in gross

94   morphology over time. Prior studies of evolutionary rates in holosteans [32], lungfishes [14,17,33],

95   and coelacanths [18–20,33] focus on different aspects of phenotype using contrasting analytical

96   tools that limit comparisons. Here, we examine the evolution of discrete (i.e., cladistic characters)

97   and continuous (i.e., body shape) traits in these three groups in a common framework to address

98   whether these examples of living fossils show similar patterns of phenotypic change over time.

99

100   2. Materials and Methods

101   (a) Discrete Character Matrices

102   We used published morphological character matrices to simultaneously infer time-scaled

103   phylogenetic hypotheses and rates of discrete-trait evolution in coelacanths, lungfishes, and

104   holosteans (see Phylogenetic Analyses). Our analyses of shape evolution within a model-fitting

105   framework then used these phylogenetic hypotheses. The source character matrices are described

106   below. For all matrices, we collapsed ambiguous or polymorphic character states to question marks

107   (?) prior to running new phylogenetic analyses.

108   For coelacanths, we used the matrix from Toriño et al. [34], a descendant of the matrix presented

109   by Forey [18] and one which has been used, with modest modifications, in a series of additional

110   studies [35–37]. The matrix contains 50 taxa (48 coelacanths) scored for 110 unordered characters,

111   87 of which are cranial and 23 of which are postcranial (inclusive of scales).

112   For lungfishes, most character matrices focus on either Devonian [38,39] or post-Devonian [40,41]

113   taxa, with few offering dense taxonomic sampling over the entire evolutionary history of the group

114   [14,21,42,43]. From the available matrices, we selected Lloyd et al. [14], which represents a

115   'supermatrix' combining datasets from several studies [38–40,44]. This matrix formed the basis

116   of a relatively recent assessment of evolutionary rates in lungfishes [14], permitting direct

117   comparison with our results obtained from a different analytical approach. This matrix contains 86

118   taxa (85 lungfishes) scored for 91 characters, 82 of which are cranial and 9 of which are postcranial

119   (inclusive of scales).

120   For holosteans, we used the dataset from López-Arbarello and Sferco [45] that includes a broad

121   sample of holosteans and other crown neopterygians. It contains 70 taxa (39 holosteans) scored

122   for 339 characters, 192 of which are cranial and 145 of which are postcranial (inclusive of scales

123   and dermal elements).

124

125   (b) Phylogenetic Analyses

126   We performed bayesian phylogenetic analyses for the lungfish, coelacanth, and holostean

127   morphological datasets in BEAST v2.6.5 [46,47]. We applied the Fossilized Birth-Death (FBD)

128   approach, which uses extinct taxa as informative tips and simultaneously estimates relationships,

129   branch durations, and rates of morphological change through time [48,49]. Empirical studies and

130   simulations show that use of the FBD prior generally results in estimated divergence times that are

131   more closely in agreement with the fossil record over other tree inference models [50–53]. We

132   used a Lewis MK model [54] with 4-category gamma distributions and a relaxed lognormal clock

133   for morphological traits. Relative to the default settings in BEAST, we changed two priors

134   specifically for coelacanths and one additional prior across all groups. In coelacanths, the two

135   priors were the *diversificationRateFBD* (Log Normal; upper = 10) and the *ucldMean* (Log Normal

136   distribution; initial = 0.1; M = 1.0; S = 1.25). Across all three groups, the *originFBD* prior was the

137   only additional change. For both sarcopterygian lineages, we set the initial search to 425 Ma

138   (Uniform distribution, upper bound of 440 Ma), which we selected based on the age range

139   estimates of the most recent common ancestor (MRCA) between sarcopterygians and

140   actinopterygians (*Guiyu* from the late Silurian [55]). For holosteans, we set the initial search to

141   260 Ma (Uniform distribution, upper bound of 423 Ma), which we selected based on the MRCA

142   for the group. All remaining FBD priors apart from those specified individually per clade above

143   were left in their default settings—Uniform for the *diversificationRateFBD* (initial = 0.01; upper

144   = infinity), *samplingProportionFBD* (initial = 0.5; upper = 1.0), *turnoverFBD* (initial = 0.5; upper

145   = 1.0), and *ucldMean* (initial = 1.0; upper = infinity); Exponential for the *gammaShape* (initial =

146   1.0; mean = 1.0); and Gamma for the *ucldStdev* (initial = 0.1; alpha = 0.5396; beta = 0.3819). We

147   did this to reduce biases associated with the *ad hoc* adjustment of informative priors by limiting

148   their use to "realistic" mechanistic models at the root search [56].

149   We applied a small set of constraints to our analyses. Topological constraints included: (1) rooting

150   using a designated outgroup (actinopterygians for coelacanths, *Psarolepis* for lungfishes, and

151   *Pteronisculus* for holosteans), (2) monophyly of the apomorphic Paleozoic coelacanths

152   *Allenypterus* and *Holopterygius* [35], (3) monophyly of a well-supported subset of total-group

153   Lepidosireniformes for lungfishes (*Gosfordia truncata*, *Lepidosiren paradoxa*, *Protopterus*

154   *annectens*, and *Ptychoceratodus serratus*) [41]. Temporal constraints included: (1) a fossil

155   calibration minimum at 100 Ma for the node representing the MRCA of *Lepidosiren paradoxa* and

156   *Protopterus annectens* based on the breakup of Gondwana [57–59] and (2) a calibration setting a

157   minimum age of divergence between *Lepiososteus* and *Atractosteus* at 93 Ma, based on the first

158   occurrence of fossil *Atractosteus* in the early Late Cretaceous [60]. We ran the phylogenetic

159   analyses for 500 million generations, with trees sampled every 100,000 generations. We used

160   Tracer v1.7 [61] to assess convergence visually via the trace plot and effective sample size (ESS)

161   calculations. We then used the TreeAnnotator utility packaged with BEAST to ignore the first 10%

162   of the trees sampled as burn-in fraction and use the post burn-in trees to generate MCC consensus

163   trees (leaving the full posterior sample files unedited). Because our downstream analyses

164   considered only those tips assigned to each total group of interest (e.g., coelacanths, lungfishes,

165   and holosteans), we pruned other clades from both the MCC tree and the trees sampled from the

166   posterior.

167   We compiled age constraints for fossil taxa at the finest level possible (typically geologic stage

168   [62–64]), drawing from a combination of original descriptions, revisions, and other resources (e.g.,

169   The Paleobiology Database, https://paleobiodb.org/). In BEAUTi v. 2.6.5 [47], the age prior for

170   each extinct taxon was set as a uniform distribution. The upper and lower boundaries are defined

171   by the age estimates for the most restrictive stratigraphic bin identified for each fossil taxon.

172   Likewise, if there was more than one fossil from different deposits or localities representing the

173   taxon, we used the most restrictive bin that accounted for its overall stratigraphic extent. We then

174   linked age priors for taxa deriving from the same geological horizon (typically a well-known fossil

175   site or formation) using the R package *palaeo* [65] to generate an XML code block that would be

176   appended manually to the BEAUTi input file used to initialise BEAST. This enforced matching

177   ages for fossils from the same deposits when running phylogenetic analyses and represents a novel

178   incorporation of stratigraphic uncertainty in a comparative framework.

179

180   (c) Evolution in Discrete Characters

181   Any outgroup taxa used to root the trees during the BEAST runs (including all Teleostei for the

182   holostean tree) were excluded from summaries of evolutionary rate in discrete characters. All

183   subsequent steps in the rate analysis pipeline used the packages *phytools* [66]*, ape* [67], and *coda*

184   [68], along with an adjusted script from Close et al. [69] calling an additional function from

185   *OutbreakTools* [70] in R v3.6.1 [71]. We began by reading the entire posterior distribution of trees

186   generated during the BEAST analysis into R, removing 10% of trees as burn-in, taking a random

187   sample of 100 trees, confirming ESS values, and then estimating per-branch rates of phenotypic

188   evolution from this subset of trees. We plotted branches from each of the sampled trees according

189   to their lengths (horizontal axis, millions of years) and rates (vertical axis, natural log scale) to

190   depict a "rate cloud". We then imported the MCC tree and used it to add a generalised loess line

191   by calculating a local average rate across lineages in million-year steps. Our overall depiction,

192   therefore, represents the average natural log rate change across time for the entire clade ([69]:

193   figure 4).

194   In addition to variation in rates of change over time, we evaluated character saturation levels within

195   all three groups using their respective morphological matrices. Prior research has investigated

196   saturation to estimate if convergence in character states is more likely than the generation of new

197   character states [72–75]. This was achieved by comparing pairwise character-state dissimilarity

198   and plotting it against patristic morphological distance (*distance_metric* = "mord") [76]. In these

199   analyses, if the average value (loess curve) increases linearly, it indicates persistent generation of

200   novel traits. However, if the average value asymptotes, it signals lineages reaching character

201   exhaustion with increased incidence of homoplasy. These analyses illustrate the relative

202   contributions of innovation and homoplasy to overall change. Although there may be limitations

203   in this method due to the coding of autapomorphic characters, potential mitigations would require

204   estimation of saturation from model-based inferences of character states, which is beyond the

205   scope of the present study.

206   The code and data used to run all subsequent analyses will be available on GitHub and archived

207   on Dryad upon acceptance of the manuscript.

208

209   (d) Morphological Landmarking Schemes

210   We selected landmarks based on previous publications with adjustments made on a per-clade basis

211   to capture homologous aspects of cranial and postcranial anatomy (see clade information below).

212   All semi-landmarks were spread out evenly beginning at the rostrum, following the dorsal body

213   line including the fleshy part of any fins, curving at the fleshy posterior end of the caudal fin, and

214   then proceeding ventrally while tracing the fleshy part of any additional fins, and then ending at

215   the posteriormost contact of the lower jaw with the ventral body line. We did not use a consistent

216   number of semi-landmark points between fixed landmarks; rather, the total semi-landmarks varied

217   depending on the topological complexity of the region they were outlining. Non-identical

218   constellations of fixed landmarks for the three lineages reflected important differences in the

219   number and arrangement of median fins. The full landmarking schemes for each clade are

220   discussed below and figured in the electronic supplementary material.

221   The arrangement of fixed landmarks for coelacanths matches that used by Friedman and Coates

222   [35], with 8 landmarks capturing fin position and 6 landmarks capturing cranial features (14 total,

223   electronic supplementary material, figure S4). 155 additional semi-landmarks were placed to

224   capture the outline of the body along segments beginning at the anteriormost tip of the skull and

225   tracing the head (one curve, 25 semi-landmarks); the dorsal region, including tracing around the

226   fleshy area of each fin lobe (four curves, 35 semi-landmarks); the fleshy dorsal and ventral regions

227   of the caudal fin (two curves, 60 semi-landmarks); and the entire ventral region, including tracing

228   around the fleshy area of each ventral midline fin, ending posteriorly at the lower jaw (two curves,

229   35 semi-landmarks).

230   The landmarking scheme for lungfishes was built to closely match the configuration of the

231   coelacanth scheme, resulting in 5 landmarks capturing fin position and 6 landmarks capturing

232   variations in skull morphology (11 total, electronic supplementary material, figure S5). The

233   reduced number of fixed cranial landmarks reflects the absence of median fin divisions in all

234   lungfishes; these divisions remain apparent in coelacanths with the most divergent postcranial

235   anatomy [35]. 115 additional semi-landmarks were placed to capture the outline of the body along

236   segments beginning at the anteriormost tip of the skull and tracing the head (one curve, 15 semi-

237   landmarks), the entire dorsal region, including tracing around the fleshy area of each fin lobe,

238   extending to the posterior tip of caudal fin (two curves, 50 semi-landmarks), the entire ventral

239   region, including tracing around the fleshy area of each ventral midline fin, ending at the lower

240   jaw (two curves, 50 semi-landmarks).

241   The landmarking scheme for holosteans descends from that used in Clarke et al. [77] and Clarke

242   and Friedman [32], with 8 landmarks capturing fin position and 6 landmarks capturing variation

243   in skull morphology (14 total, electronic supplementary material, figure S6). 120 additional semi-

244   landmarks were placed to capture the outline of the body along segments beginning at the

245   anteriormost tip of the skull and tracing the head (one curve, 25 semi-landmarks); the dorsal region,

246   including tracing around the fleshy area of each fin (four curves, 55 semi-landmarks); the fleshy

247   dorsal and ventral regions of the caudal fin (two curves, 20 semi-landmarks), and the entire ventral

248   region, including tracing around the fleshy area of each ventral midline fin, ending posteriorly at

249   the lower jaw (one curve, 20 semi-landmarks).

250

251   (e) Body Shape Analyses

252   We landmarked a combination of original specimen photographs, published fossil images, and

253   technical illustrations for species that were present in our phylogenetic analyses. The final dataset

254   consisted of 27 coelacanths, 16 lungfishes, and 62 holosteans. Each taxon was then landmarked

255   according to the schemes outlined above and their body shape was traced with spline curves in R

256   v3.6.1 [71] using the package *StereoMorph* (*digitizeImages*) [78]. The unaligned landmark and

257   semi-landmark coordinates were imported using the package *geomorph* [79,80] (*readland.shapes*,

258   adapting the total semilandmarks on a per-curve basis to be dense enough to capture fin details as

259   detailed above), adjusted with a Procrustes transformation (*gpagen*), and transformed using a

260   principal components analysis (PCA) and phylogenetically-aligned components analysis (PaCA)

261   (both via *gm.prcomp*). Morphospace plots for all taxa can be found in electronic supplementary

262   material figures S4–S6.

263

264   (f) Fitting Evolutionary Models of Continuous Trait Evolution

265   We fit three alternative models of continuous trait evolution to body shape datasets for each clade

266   using the R package mvMORPH [81], taking advantage of new approaches for investigating high-

267   dimensional morphometric datasets [82]. For each clade, we fit: (1) Brownian Motion (BM), (2)

268   Ornstein-Uhlenbeck (OU), and (3) Accelerating-Decelerating (ACDC) models. BM reflects a

269   constant accumulation of shape disparity over time; OU models a central tendency, which is

270   interpreted biologically as an adaptive peak or evolutionary constraint [83,84]; and ACDC reflects

271   accelerating or decelerating exponential rates of change over the history of a clade [81,85]. Early

272   Burst (EB) is a special case within the ACDC framework where rates exclusively decelerate

273   [24,81,85]. EB was originally formulated as a model of adaptive radiation [24], but it also matches

274   patterns sometimes inferred for living fossils [14,17]. For the purposes of our analyses, we refer

275   to the exponential models inferring declining rates as EB.

276   We fit the three alternative models using the *mvgls* function in mvMORPH. We opted for the

277   penalised likelihood approach in *mvgls* because it is designed to operate directly on highly

278   dimensional morphometric datasets and can efficiently optimise multivariate models with

279   hundreds of variables [82]. Additionally, other likelihood models can lead to, for example,

280   exaggerated estimates of the exponential parameter *b* in likelihood (e.g., *mvEB*) versus penalised

281   likelihood (e.g., *mvgls*) model fitting analyses [82]. The *mvgls* flags we used across all analyses

282   were *scale.height* = F, *method* = "PL-LOOCV", *penalty* = "RidgeArch", *target* = "unitVariance",

283   and *error* = T. The error option estimates an extra nuisance parameter intended to account for

284   variation not explained by the model (e.g., measurement error) and is recommended for empirical

285   datasets [82,86].

286   To run the analyses, we used the MCC tree as an initial phylogenetic framework and all PC axes—

287   those explaining 100% of the variation—for each taxon (24, 15, and 60 total axes for coelacanths,

288   lungfishes, and holosteans, respectively). To account for variation in model fit as a function of

289   uncertainty in tree topology and evolutionary timescale, we repeated the procedure using a sample

290   of 100 trees from the posterior distribution of trees generated by the BEAST analyses. We

291   calculated GIC scores [82,87,88] and weights for each model fit across all sampled trees, and

292   visualised the resulting distributions (figures 1*c*, 2*c*, 3*c*; GIC scores in the electronic supplementary

293   material).

294   We also performed parametric bootstrapping—using only the parameters from the best fit model

295   per clade—to explore our results more thoroughly. The empirical parameters for the *mvSIM*

296   function were thus derived from *mvgls* model fitting using the unit-scaled MCC tree and the PC

297   axes explaining 100% of the variance. Due to optimization issues, holosteans required the *mvgls*

298   parameter under *model* = "EB" to be estimated using *REML* = FALSE throughout. Coelacanths

299   and lungfishes showed no optimization issues and used the default *REML* = TRUE. We then

300   performed bootstrapping on 100 *mvSIM* replicates, with the upper and lower bounds of parameter

301   search space iteratively increased if model fitting reached the default parameter limits. We plotted

302   the distribution of the parameter for each best fit model estimated from these bootstrapped datasets

303   per group (electronic supplementary material, figure S8) and calculated the 95% confidence

304   interval.

305

306   **3. Results**

307   (a) Phylogenetic Relationships and Evolutionary Timescales

308   Our Bayesian analyses using a Fossilised Birth-Death prior produced phylogenetic topologies that

309   correspond closely to those reported from prior analyses of the same matrices. Our estimated ages

310   of last common ancestor of all sampled lineages for each of our groups are: Silurian for coelacanths

311   (428 Ma; 95% HPD: 415–446 Ma; electronic supplementary material, figure S1) and lungfishes

312   (432 Ma; 95% HPD: 425–435 Ma; electronic supplementary material, figure S2), and early

313   Permian for holosteans (288 Ma; 95% HPD: 272–307 Ma; electronic supplementary material,

314   figure S3). Most nodes within the holostean and coelacanth phylogenies have relatively high clade

315   credibility values (>75%). Posterior support for most nodes in the lungfish tree is considerably

316   lower, reflecting a longstanding pattern of heterogeneous topologies recovered in phylogenetic

317   studies of the group (e.g., [42]). Further discussion and complete maximum clade credibility

318   (MCC) trees can be found in the electronic supplementary material.

319

320   (b) Discrete Character Evolution

321   For coelacanths, rates of discrete character evolution show an overall decline from the origin of

322   the clade to the present (figure 1*a*). Modest peaks in evolutionary rates occur during the Early

323   Devonian, Permian, and Early Triassic, with rates dropping substantially by the end of the Triassic.

324   Rates plateau during the Jurassic before dropping precipitously by the end of the Cretaceous. A

325   nearly linear relationship between morphological disparity and patristic distances indicates little

326   character saturation (figure 1*b*).

327   For lungfishes, rates of discrete character evolution show an overall decline from the origin of the

328   clade to the present (figure 2*a*). The highest rates occur in the Silurian and Early Devonian, but

329   these decline into the Late Devonian. At this point, they stabilise for the duration of the Paleozoic.

330   Rates decline monotonically throughout the Mesozoic and Cenozoic. An apparent asymptote in

331   values of morphological dissimilarity with increasing patristic distance indicates some saturation

332   of character states (figure 2*b*).

333   For holosteans, rates of discrete character evolution show irregular but modest fluctuations about

334   a relatively constant rate over time (figure 3*a*). Distinct peaks in rates of morphological evolution

335   were recovered in the Triassic and Early Cretaceous, each followed by a nearly equal and opposite

336   decrease in rates. From the Late Cretaceous onward, rates remain approximately constant.

337   Dissimilarity increases sharply as the patristic distance increases at relatively low patristic

338   distances. Slower accumulation at higher patristic distances indicates some character saturation

339   (figure 3*b*). Discrete patterns are summarised for all three lineages in electronic supplementary

340   material, table S1.

341

342   (c) Body Shape Evolution

343   Landmarking schemes and shape spaces for the three lineages are summarised in electronic

344   supplementary material, figures S4–S6. For coelacanths, 24 principal component (PC) axes

345   summarised 100% of body shape variance, with over 70% captured by the first two axes. PC1

346   reflects variation in the anterior extension of the epichordal/hypochordal lobes of the caudal fin

347   (48% of total variance) and PC2 summarises differences in body depth (23% of total variance)

348   (electronic supplementary material, figure S4). PC3 and PC4 capture head shape, pelvic fin

349   placement, and posterior body shape (14% of total variance, cumulatively). All further axes

350   summarise minor variations relating to the median fins. The best-fit model on the MCC tree was

351   the Accelerating-Decelerating (ACDC) model with declining rates of change, corresponding to the

352   Early Burst (EB) variant (Generalised Information Criterion [82,87,88] weight [GICw] = 1)

353   (figure 1*c*; electronic supplementary material, figure S7, table S2). Estimated *b*—representing the

354   exponential change in evolutionary rate—for empirical data on the unit-scaled MCC tree was

355   strongly negative (*b* ~ -10.7; 95% CI from parametric bootstrapping: -20.3, -8.99; electronic

356   supplementary material, figure S8). This estimate implies a substantial decrease in rates of

357   approximately four orders of magnitude at the tips compared to those at the root.

358   For lungfishes, 15 PC axes summarised 100% of body shape variance, with 69% captured by the

359   first two axes. PC1 reflects differences in the dorsal extent and anterior reach of the epichordal

360   lobe (52.6% of total variance) and PC2 indicates the anterior extension and separation of the dorsal

361   fin or fins as well as the extent of the anal fin (16.5% of variance) (electronic supplementary

362   material, figure S5). PC3 and PC4 capture two aspects of body depth (extension and compression,

363   respectively; 18% of total variance, cumulatively). Subsequent axes summarised more subtle

364   differences between fin placement, head length, and body length. The best-fit evolutionary model

365   was ACDC (GICw ~ 0.52), although this is not decisive due to alternative models we evaluated

366   receiving moderate support (Ornstein-Uhlenbeck [OU]: GICw ~ 0.34; Brownian motion [BM]:

367   GICw ~ 0.14) (figure 2*c*; electronic supplementary material, table S3). Additionally, some of our

368   results show slightly higher support for OU in fitted posterior trees when ACDC was not the

369   preferred model (figure 2*c*). Estimated *b* was negative (*b* ~ -3.85; 95% CI from parametric

370   bootstrapping: -24.3, -0.91; electronic supplementary material, figure S8), corresponding to the

371   EB case of ACDC. This value represents an order of magnitude decline in rates, with those at the

372   youngest tips 2% of that at the root. Although the confidence interval for the bootstrapped values

373   does not include zero, some replicates estimated a positive *b*, indicating an inability to distinguish

374   EB from BM (electronic supplementary material, figure S8).

375   For holosteans, 60 PC axes summarised 100% of body shape variation, with 63% of the variance

376   summarised by the first two axes. PC1 captures the anterior-posterior position of the dorsal fin

377   (35.6% of total variance), and PC2 reflects body depth (27.2% of variance) (electronic

378   supplementary material, figure S6). PC3 and PC4 indicate dorsal and caudal fin form and

379   placement, and dorsal or ventral body curves (together 16.9% of total variance). Further axes

380   summarised differences in snout and head length, fin placement, and body shape. The best-fit

381   evolutionary model was ACDC (GICw ~ 0.90) (figure 3c; electronic supplementary material, table

382   S4). Estimated b was weakly negative (b ~ -0.27; 95% CI from parametric bootstrapping: -1.65,

383   0.44, electronic supplementary material, figure S8), indicating a minor decrease where the rates at

384   the youngest tips are ~76% of those at the base of the tree. The distribution of b generated by

385   parametric bootstrapping includes zero, which signifies difficulty differentiating between

386   changing versus constant rates (a pattern more readily apparent in the nearly identical plots of GIC

387   scores for holosteans, electronic supplementary material, figure S7).

388

389   4. Discussion and Conclusions

390   (a) Comparison with Previous Interpretations of Phenotypic Evolution in Living Fossil Lineages

391   Our results provide a reexamination of previous interpretations of phenotypic evolution in

392   coelacanths, lungfishes, and holosteans. While these groups are commonly thought to exhibit

393   specific types of morphological change, the degree to which these evolutionary trajectories have

394   been quantified varies substantially. Patterns in lungfishes are perhaps the most well-established

395   as they benefit from a long pedigree of research, beginning with Westoll's [17] formative study

396   quantifying the accumulation of "modern" traits in fossil lungfishes. That study and those that

397   followed [14,21,32] support high rates of change in discrete traits at the root of lungfish phylogeny

398   followed by a pronounced decline over the group's history. Our results broadly corroborate these

399   findings. In contrast to studies of evolutionary rate in discrete characters, there are no quantified

400   assessments of body-shape evolution in lungfishes. Nevertheless, there is a strong informal

401   argument in the literature—tracing back to at least Dollo [89]—that the most substantial changes

402   to lungfish body shape occurred early in the group's Devonian history, associated with the origin

403   of a single, continuous median fin [32,90,91]. However, we do not find overwhelmingly strong

404   support for declining rates of body shape evolution in lungfishes, with constant-rate alternatives

405   having a combined GICw ~0.48. The lungfish shape dataset is the smallest for the three lineages

406   considered ($n = 16$, versus 27 coelacanths and 62 holosteans). This sample size is a limitation of

407   the lungfish record [35,89–91] and it is possible additional discoveries of articulated material could

408   increase support for a model with high early rates of change (e.g., EB) for the group.

409   Quantitative investigation of phenotypic evolution in coelacanths began with Schaeffer's [33]

410   comparative analysis of the group alongside lungfishes. Inspired by and building on Westoll's [17]

411   approach, Schaeffer [33] identified similar patterns for lungfishes and coelacanths: a Devonian

412   peak in rates of change followed by a rapid decay. Using a more extensive set of taxa and characters

413   in an explicitly phylogenetic framework, Cloutier [20] reported a broadly similar pattern with three

414   different measures of evolutionary rate. Forey [18] provided a coarse overview of accumulated

415   changes across coelacanth phylogeny between arbitrary stratigraphic intervals, showing a net

416   decline in steps over time. In line with these previous estimates, we find a decrease in rates of

417   discrete character evolution in coelacanths, punctuated by modest increases in the latest Paleozoic

418   and earliest Mesozoic. Interestingly, the most consistent interval of declining rates in coelacanths

419   begins in the early Triassic, preceding their peak in lineage diversity later in that period [18]

420   (electronic supplementary material, figure S1). Thus, it appears that the onset of low rates of

421   change preceded a decline in taxonomic diversity. Whether or not this inference is affected by

422   variability in sampling over time is an unavoidable potential source of bias when examining

423   lineages that become depauperate over time. Nevertheless, our results add further detail to this

424   picture by showing that coelacanths consistently developed new traits even as their overall rates

425   of change declined over time. As with lungfishes, no quantitative assessments of coelacanth

426   evolutionary rates are based on shape. However, Schaeffer ([33]: figure 1) implied extreme

427   conservatism in body form consistent with low rates of change. Friedman and Coates [35]

428   suggested that high morphological disparity early in coelacanth history could stem from elevated

429   evolutionary rates that subsequently declined. Our comparative analyses strongly support this

430   latter interpretation, which indicates a substantial decline in rates of body-shape evolution in

431   coelacanths over their history.

432   Holosteans are central to the concept of living fossils, but there are few quantitative assessments

433   of phenotypic evolution in the group. Clarke et al. [77] compared patterns of body shape evolution

434   between early holosteans and teleosts, finding no consistent differences in rate between the groups

435   when considering phylogenetic uncertainty. This prior study did not test for variable evolutionary

436   rates within holosteans, and there is no strong prior hypothesis for patterns within the group beyond

437   qualitative assessments based on close phenotypic correspondence between living holosteans

438   relative to their closest fossil relatives. Clarke et al. [77] did investigate the degree of constraint in

439   holostean body shape relative to null models using Bloomberg's K, and suggested that body shape

440   evolution in holosteans is substantially more constrained than that expected under Brownian

441   motion. Clarke and Friedman [32] later reported relatively static levels of morphological disparity

442   over the first 150 million years of holostean history, consistent with myriad modes of phenotypic

443   change, including evolutionary constraint [92]. Although our examination of character saturation

444   for holosteans suggests some degree of constraint for discrete characters, we find that OU is the

445   least well supported of the models considered for holostean shape data.

446

447   (b) Inconsistent Evolutionary Patterns among and within Living Fossil Lineages

448   Systematic paleobiologists often infer processes or modes of phenotypic evolution from subsets of

449   an organism's overall anatomy. However, different aspects of morphology can show divergent

450   macroevolutionary patterns, suggesting that mosaic evolution of phenotypes is widespread

451   [30,92]. Therefore, we aimed to summarise the overall anatomy of our focal lineages across two

452   datasets—discrete characters and overall body shape—which has provided an opportunity to

453   examine the degree to which different aspects of phenotype show corresponding or divergent

454   patterns of change. Our unified approach helps to more fully understand the living fossil concept,

455   which has historically been evaluated using independent measures of phenotype. Contrasting

456   approaches and varied anatomical subsets can be found not only in the literature examining our

457   focal clades, but also in groups as taxonomically distant as horseshoe crabs [13] and tuataras [15],

458   where declining disparity and rates over time, respectively, have been recovered for those groups

459   independently.

460   Two important conclusions emerge from our analyses. First, there does not appear to be a single

461   pattern of morphological evolution universally shared *among* these lineages. Although there is

462   some evidence for declining rates when assessing both discrete-trait and shape evolution separately

463   for all three groups, both the support for, and magnitude of, this decline shows substantial

464   differences among the lineages. Second, and perhaps equally important, different aspects of

465   morphology (i.e., discrete characters and shape) do not imply similar underlying processes *within*

466   each lineage, even though each data type might be thought of as independently, and broadly,

467   summarising overall organismal morphology.

468   We observe a close correspondence between discrete and continuous trait evolution in coelacanths

469   (Table S1). Rates of discrete-character evolution show a first-order pattern of decline over time;

470   body shape is likewise best fit by a declining-rates ACDC (i.e., EB) model, and parameter

471   estimates imply a reduction of rates by several orders of magnitude over coelacanth history.

472   Patterns of character saturation for coelacanths suggest continued innovation throughout the

473   clade's history, suggesting few constraints on the evolution of discrete traits (consistent with

474   persistent diffusion through trait space), although at ever-decreasing rates. Likewise, evolutionary

475   patterns across both morphological datasets in holosteans are highly congruent (Table S1). Rates

476   of discrete-character evolution are remarkably constant over time, with only a modest decline over

477   their entire history. Patterns of shape evolution broadly mirror this, with estimated values of *b*

478   suggesting only minor changes in evolutionary rates throughout clade history.

479   Lungfishes present an alternative case. Like coelacanths, their rates of discrete character evolution

480   decline substantially over time yet, in contrast, lungfishes appear to evolve in a more constrained

481   fashion with more pronounced character saturation. Although the EB case of ACDC is the

482   favoured model for body shape evolution in lungfishes, this is not decisive given its weak support

483   (GICw ~ 0.52) combined with parameter estimates that imply a modest rate reduction over time

484   in comparison to coelacanths (Table S1).

485   Phenotypically, lungfishes, coelacanths, and holosteans illustrate attributes commonly ascribed to

486   living fossils [7]: extant species closely resemble some ancient taxa. However, it has long been

487   clear that superficially similar patterns like these can arise from contrasting dynamics of

488   evolutionary change [93]. Phylogenetic information is crucial for distinguishing between

489   alternative mechanisms underlying otherwise comparable phenotypic patterns [94]. By employing

490   a common phylogenetic comparative framework, we sought to determine whether the similarities

491   among three canonical living fossil groups reflected shared aspects of phenotypic evolution or

492   whether contrasting processes yielded superficially similar morphological patterns. We find

493   differences in the support for distinct evolutionary models inferred across—and in some cases

494   within—these living fossil lineages. Thus, as with other quantitative assessments of phenotypic

495   diversification across clades [24], we find that shared features ascribed to living fossils can arise

496   from distinct histories of evolutionary change. We anticipate that a broader approach will lead to

497   better characterization of such groups [29], contributing to a better understanding of the origin and

498   persistence of living fossils and other phylogenetic relics [8].

499

Ethics

This work did not require ethical approval from a human subject or animal welfare committee.

Data Accessibility

Following acceptance, all code and data will be available in the Dryad Digital Repository and on Github.

Authors' contributions

R.A.R.-V.: conceptualization, data curation, formal analysis, investigation, methodology, software, validation, visualisation, writing – original draft, writing – review & editing;

J.S.B: formal analysis, methodology, software, validation, visualisation, writing – original draft, writing – review & editing;

J.T.C.: data curation, validation, writing – original draft, writing – review & editing;

M.F.: conceptualization, investigation, methodology, supervision, validation, writing – original draft, writing – review & editing.

All authors gave final approval for publication and agreed to be held accountable for the work performed herein.

518 **Declaration of AI use**

519 We have not used AI-assisted technologies in creating this article.

520

521 **Competing interests**

522 We declare we have no competing interests.

523

524 **Funding**

532

533 **Acknowledgements**

537

538 **Footnotes**

539 Electronic supplementary material have been uploaded alongside this preprint. Following

540 acceptance, final electronic supplementary materials will be available online at the publisher's

541 website.

542

References

1. Darwin CR. 1859 *On the Origin of Species by Means of Natural Selection, or the Preservation of Favoured Races in the Struggle for Life*. London: John Murray.

2. Eldredge N, Stanley SM. 1984 *Living Fossils*. New York: Springer Verlag.

3. Casane D, Laurenti P. 2013 Why coelacanths are not 'living fossils'. *BioEssays* **35**, 332–338. (doi:10.1002/bies.201200145)

4. Watkins A. 2021 The Epistemic Value of the Living Fossils Concept. *Philos. Sci.* **88**, 1221–1233. (doi:10.1086/714875)

5. Grandcolas P, Nattier R, Trewick S. 2014 Relict species: a relict concept? *Trends Ecol. Evol.* **29**, 655–663. (doi:10.1016/j.tree.2014.10.002)

6. Lidgard S, Love AC. 2018 Rethinking Living Fossils. *BioScience* **68**, 760–770. (doi:10.1093/biosci/biy084)

7. Lidgard S, Love AC. 2021 The living fossil concept: reply to Turner. *Biol. Philos.* **36**, 13. (doi:10.1007/s10539-021-09789-z)

8. Turner DD. 2019 In defense of living fossils. *Biol. Philos.* **34**, 23. (doi:10.1007/s10539-019-9678-y)

9. Werth AJ, Shear WA. 2014 The Evolutionary Truth About Living Fossils. *Am. Sci.* **102**, 434–443.

10. Schopf TJM. 1984 Rates of Evolution and the Notion of 'Living Fossils'. *Annu. Rev. Earth Planet. Sci.* **12**, 245–292. (doi:10.1146/annurev.ea.12.050184.001333)

11. Fisher DC. 1990 Rates of Evolution – Living Fossils. In *Paleobiology: a Synthesis* (eds DEG Briggs, PR Crowther), pp. 152–159. London, UK: Blackwell Scientific.

12. Cavin L, Guinot G. 2014 Coelacanths as 'almost living fossils'. *Front. Ecol. Evol.* **2**, 1–5. (doi:10.3389/fevo.2014.00049)

13. Bicknell RDC *et al.* 2022 Habitat and developmental constraints drove 330 million years of horseshoe crab evolution. *Biol. J. Linn. Soc.* **136**, 155–172. (doi:10.1093/biolinnean/blab173)

14. Lloyd GT, Wang SC, Brusatte SL. 2011 Identifying heterogeneity in rates of morphological evolution: discrete character change in the evolution of lungfish (Sarcopterygii; Dipnoi). *Evolution* **66**, 330–348. (doi:10.1111/j.1558-5646.2011.01460.x)

15. Simões TR, Caldwell MW, Pierce SE. 2020 Sphenodontian phylogeny and the impact of model choice in Bayesian morphological clock estimates of divergence times and evolutionary rates. *BMC Biol.* **18**, 191. (doi:10.1186/s12915-020-00901-5)

16. Bennett DJ, Sutton MD, Turvey ST. 2018 Quantifying the living fossil concept. *Palaeontol. Electron.* **21**. (doi:10.26879/750)

17. Westoll TS. 1949 On the evolution of the Dipnoi. In *Genetics, Paleontology and Evolution* (eds GL Jepsen, E Mayr, GG Simpson), pp. 121–184. Princeton, NJ: Princeton University Press.

18. Forey PL. 1998 *History of the Coelacanth Fishes*. Chapman & Hall.

19. Forey PL. 1988 Golden jubilee for the coelacanth *Latimeria chalumnae*. *Nat. Rev.* **336**, 727–732.

20. Cloutier R. 1991 Patterns, trends, and rates of evolution within the Actinistia. *Environ. Biol. Fishes* **32**, 23–58. (doi:10.1007/BF00007444)

21. Cui X, Friedman M, Qiao T, Yu Y, Zhu M. 2022 The rapid evolution of lungfish durophagy. *Nat. Commun.* **13**, 2390. (doi:10.1038/s41467-022-30091-3)

22. Uyeda JC, Zenil-Ferguson R, Pennell MW. 2018 Rethinking phylogenetic comparative methods. *Syst. Biol.* **67**, 1091–1109. (doi:10.1093/sysbio/syy031)

23. Herrera-Flores JA, Stubbs TL, Benton MJ. 2017 Macroevolutionary patterns in Rhynchocephalia: is the tuatara (*Sphenodon punctatus*) a living fossil? *Palaeontology* **60**, 319–328. (doi:10.1111/pala.12284)

24. Harmon LJ *et al.* 2010 Early bursts of body size and shape evolution are rare in comparative data. *Evolution* (doi:10.1111/j.1558-5646.2010.01025.x)

25. Miles DB, Ricklefs RE, Losos JB. 2023 How exceptional are the classic adaptive radiations of passerine birds? *Proc. Natl. Acad. Sci.* **120**, e1813976120. (doi:10.1073/pnas.1813976120)

26. Givnish TJ. 2015 Adaptive radiation versus 'radiation' and 'explosive diversification': why conceptual distinctions are fundamental to understanding evolution. *New Phytol.* **207**, 297–303. (doi:10.1111/nph.13482)

27. Osborn HF. 1902 The Law of Adaptive Radiation. *Am. Nat.* **36**, 353–363.

28. Schluter D. 2000 *The ecology of adaptive radiation*. Oxford: Oxford University Press.

29. Simões M, Breitkreuz L, Alvarado M, Baca S, Cooper JC, Heins L, Herzog K, Lieberman BS. 2016 The Evolving Theory of Evolutionary Radiations. *Trends Ecol. Evol.* **31**, 27–34. (doi:10.1016/j.tree.2015.10.007)

30. Slater GJ, Friscia AR. 2019 Hierarchy in adaptive radiation: A case study using the Carnivora (Mammalia). *Evolution* **73**, 524–539. (doi:10.1111/evo.13689)

31. Musser AM. 2003 Review of the monotreme fossil record and comparison of palaeontological and molecular data. *Comp. Biochem. Physiol. A. Mol. Integr. Physiol.* **136**, 927–942. (doi:10.1016/S1095-6433(03)00275-7)

32. Clarke JT, Friedman M. 2018 Body-shape diversity in Triassic–Early Cretaceous neopterygian fishes: sustained holostean disparity and predominantly gradual increases in teleost phenotypic variety. *Paleobiology* **44**, 402–433. (doi:10.1017/pab.2018.8)

33. Schaeffer B. 1952 Rates of Evolution in the Coelacanth and Dipnoan Fishes. *Evolution* **6**, 101. (doi:10.2307/2405507)

34. Toriño P, Soto M, Perea D. 2021 A comprehensive phylogenetic analysis of coelacanth fishes (Sarcopterygii, Actinistia) with comments on the composition of the Mawsoniidae and Latimeriidae: evaluating old and new methodological challenges and constraints. *Hist. Biol.* **33**, 3423–3443. (doi:10.1080/08912963.2020.1867982)

35. Friedman M, Coates MI. 2006 A newly recognized fossil coelacanth highlights the early morphological diversification of the clade. *Proc. R. Soc. B Biol. Sci.* **273**, 245–250. (doi:10.1098/rspb.2005.3316)

36. Dutel H, Maisey JG, Schwimmer DR, Janvier P, Herbin M, Clément G. 2012 The Giant Cretaceous Coelacanth (Actinistia, Sarcopterygii) *Megalocoelacanthus dobiei* Schwimmer, Stewart & Williams, 1994, and Its Bearing on Latimerioidei Interrelationships. *PLoS ONE* **7**, e49911. (doi:10.1371/journal.pone.0049911)

37. Cavin L, Mennecart B, Obrist C, Costeur L, Furrer H. 2017 Heterochronic evolution explains novel body shape in a Triassic coelacanth from Switzerland. *Sci. Rep.* **7**, 13695. (doi:10.1038/s41598-017-13796-0)

38. Schultze H-P, Chorn J. 1997 The Permo-Carboniferous genus *Sagenodus* and the beginning of modern lungfish. *Contrib. Zool.* **67**, 9–70.

39. Schultze H-P. 2001 *Melanognathus*, a primitive dipnoan from the Lower Devonian of the Canadian arctic and the interrelationships of Devonian dipnoans. *J. Vertebr. Paleontol.* **21**, 781–794. (doi:10.1671/0272-4634(2001)021[0781:MAPDFT]2.0.CO;2)

40. Schultze H-P. 2004 Mesozoic sarcopterygians. In *Mesozoic Fishes 3 – Systematics, Paleoenvironments and Biodiversity* (eds G Arratia, A Tintori), pp. 463–492. München: Verlag Dr. Friedrich Pfeil.

41. Criswell KE. 2015 The comparative osteology and phylogenetic relationships of African and South American lungfishes (Sarcopterygii: Dipnoi). *Zool. J. Linn. Soc.* **174**, 801–858. (doi:10.1111/zoj.12255)

42. Challands TJ, Smithson TR, Clack JA, Bennett CE, Marshall JEA, Wallace-Johnson SM, Hill H. 2019 A lungfish survivor of the end-Devonian extinction and an Early Carboniferous dipnoan radiation. *J. Syst. Palaeontol.* **17**, 1825–1846.

644   (doi:10.1080/14772019.2019.1572234)

645   43. Smithson TR, Richards KR, Clack JA. 2016 Lungfish diversity in Romer's Gap: reaction to
646   the end-Devonian extinction. *Palaeontology* **59**, 29–44. (doi:10.1111/pala.12203)

647   44. Schultze H-P, Marshall CR. 1993 Contrasting the use of functional complexes and isolated
648   characters in lungfish evolution. *Mem. Assoc. Australas. Palaeontol.* **15**, 211–224.

649   45. López-Arbarello A, Sferco E. 2018 Neopterygian phylogeny: the merger assay. *R. Soc.*
650   *Open Sci.* **5**, 172337. (doi:10.1098/rsos.172337)

651   46. Bouckaert R, Heled J, Kühnert D, Vaughan T, Wu C-H, Xie D, Suchard MA, Rambaut A,
652   Drummond AJ. 2014 BEAST 2: A Software Platform for Bayesian Evolutionary Analysis.
653   *PLoS Comput. Biol.* **10**, e1003537. (doi:10.1371/journal.pcbi.1003537)

654   47. Bouckaert R *et al.* 2019 BEAST 2.5: An advanced software platform for Bayesian
655   evolutionary analysis. *PLOS Comput. Biol.* **15**, e1006650.
656   (doi:10.1371/journal.pcbi.1006650)

657   48. Stadler T. 2010 Sampling-through-time in birth–death trees. *J. Theor. Biol.* **267**, 396–404.
658   (doi:10.1016/j.jtbi.2010.09.010)

659   49. Heath TA, Huelsenbeck JP, Stadler T. 2014 The fossilized birth-death process for coherent
660   calibration of divergence-time estimates. *Proc. Natl. Acad. Sci.* **111**, E2957–E2966.
661   (doi:10.1073/pnas.1319091111)

662   50. Arcila D, Pyron RA, Tyler JC, Ortí G, Betancur-R R. 2015 An evaluation of fossil tip-dating
663   versus node-age calibrations in tetraodontiform fishes (Teleostei: Percomorphaceae). *Mol.*
664   *Phylogenet. Evol.* **82**, 131–145. (doi:10.1016/j.ympev.2014.10.011)

665   51. Grimm GW, Kapli P, Bomfleur B, McLoughlin S, Renner SS. 2015 Using More Than the
666   Oldest Fossils: Dating Osmundaceae with Three Bayesian Clock Approaches. *Syst. Biol.*
667   **64**, 396–405. (doi:10.1093/sysbio/syu108)

668   52. Zhang C, Stadler T, Klopfstein S, Heath TA, Ronquist F. 2016 Total-Evidence Dating under
669   the Fossilized Birth–Death Process. *Syst. Biol.* **65**, 228–249. (doi:10.1093/sysbio/syv080)

670   53. Luo A, Duchêne DA, Zhang C, Zhu C-D, Ho SYW. 2019 A Simulation-Based Evaluation of
671   Tip-Dating Under the Fossilized Birth–Death Process. *Syst. Biol.* **syz038**.
672   (doi:10.1093/sysbio/syz038)

673   54. Lewis PO. 2001 A likelihood approach to estimating phylogeny from discrete morphological
674   character data. *Syst. Biol.* **50**, 913–925. (doi:10.1080/106351501753462876)

675   55. Zhu M, Zhao W, Jia L, Lu J, Qiao T, Qu Q. 2009 The oldest articulated osteichthyan reveals
676   mosaic gnathostome characters. *Nature* **458**, 469–474. (doi:10.1038/nature07855)

677   56. Matzke NJ, Wright A. 2016 Inferring node dates from tip dates in fossil Canidae: the
678   importance of tree priors. *Biol. Lett.* **12**, 20160328. (doi:10.1098/rsbl.2016.0328)

679   57. Kemp A, Cavin L, Guinot G. 2017 Evolutionary history of lungfishes with a new phylogeny of
680   post-Devonian genera. *Palaeogeogr. Palaeoclimatol. Palaeoecol.* **471**, 209–219.
681   (doi:10.1016/j.palaeo.2016.12.051)

682   58. Longrich NR. 2017 A stem lepidosireniform lungfish (Sarcopterygia: Dipnoi) from the Upper
683   Eocene of Libya, North Africa and implications for Cenozoic lungfish evolution. *Gondwana*
684   *Res.* **42**, 140–150. (doi:10.1016/j.gr.2016.09.007)

685   59. Capobianco A, Friedman M. 2019 Vicariance and dispersal in southern hemisphere
686   freshwater fish clades: a palaeontological perspective. *Biol. Rev.* **94**, 662–699.
687   (doi:10.1111/brv.12473)

688   60. Grande L. 2010 An Empirical and Synthetic Pattern Study of Gars (Lepisosteiformes) and
689   Closely Related Species, Based Mostly on Skeletal Anatomy. The Resurrection of Holostei.
690   *Copeia* **10**, 1–871.

691   61. Rambaut A, Drummond AJ, Xie D, Baele G, Suchard MA. 2018 Posterior Summarization in
692   Bayesian Phylogenetics Using Tracer 1.7. *Syst. Biol.* **67**, 901–904.
693   (doi:10.1093/sysbio/syy032)

694   62. Gradstein FM, Ogg JG, Schmitz MD, Ogg GM. 2012 *The Geologic Time Scale 2012*. 1st ed.

695   Amsterdam; Boston: Elsevier.
696   63. Ogg JG, Ogg GM, Gradstein FM. 2016 *A Concise Geologic Time Scale 2016*. Amsterdam,
697   Netherlands: Elsevier.
698   64. Gradstein FM, Ogg JG, Schmitz MD, Ogg GM. 2020 *The Geologic Time Scale 2020*.
699   Amsterdam: Elsevier.
700   65. King B, Rücklin M. 2020 Tip dating with fossil sites and stratigraphic sequences. *PeerJ* **8**,
701   e9368. (doi:10.7717/peerj.9368)
702   66. Revell LJ. 2012 phytools: an R package for phylogenetic comparative biology (and other
703   things). *Methods Ecol. Evol.* **3**, 217–223. (doi:10.1111/j.2041-210X.2011.00169.x)
704   67. Paradis E, Claude J, Strimmer K. 2004 APE: Analyses of Phylogenetics and Evolution in R
705   language. *Bioinformatics* **20**, 289–290. (doi:10.1093/bioinformatics/btg412)
706   68. Plummer M, Best N, Cowles K, Vines K. 2006 CODA: Convergence diagnosis and output
707   analysis for MCMC. *R News* **6**, 7–11.
708   69. Close RA, Johanson Z, Tyler JC, Harrington RC, Friedman M. 2016 Mosaicism in a new
709   Eocene pufferfish highlights rapid morphological innovation near the origin of crown
710   tetraodontiforms. *Palaeontology* **59**, 499–514. (doi:10.1111/pala.12245)
711   70. Jombart T *et al.* 2014 OutbreakTools: A new platform for disease outbreak analysis using
712   the R software. *Epidemics* **7**, 28–34. (doi:10.1016/j.epidem.2014.04.003)
713   71. R Core Team. 2013 R: A language and environment for statistical computing.
714   72. Wagner PJ. 2000 Exhaustion of morphologic character states among fossil taxa. *Evolution*
715   **54**, 365–386. (doi:10.1111/j.0014-3820.2000.tb00040.x)
716   73. Wagner PJ, Ruta M, Coates MI. 2006 Evolutionary patterns in early tetrapods. II. Differing
717   constraints on available character space among clades. *Proc. R. Soc. B Biol. Sci.* **273**,
718   2113–2118. (doi:10.1098/rspb.2006.3561)
719   74. Oyston JW, Hughes M, Wagner PJ, Gerber S, Wills MA. 2015 What limits the morphological
720   disparity of clades? *Interface Focus* **5**, 20150042. (doi:10.1098/rsfs.2015.0042)
721   75. Brocklehurst N, Benson RJ. 2021 Multiple paths to morphological diversification during the
722   origin of amniotes. *Nat. Ecol. Evol.* **5**, 1243–1249. (doi:10.1038/s41559-021-01516-x)
723   76. Brocklehurst N, Panciroli E, Benevento GL, Benson RBJ. 2021 Mammaliaform extinctions
724   as a driver of the morphological radiation of Cenozoic mammals. *Curr. Biol.* **31**, 2955-
725   2963.e4. (doi:10.1016/j.cub.2021.04.044)
726   77. Clarke JT, Lloyd GT, Friedman M. 2016 Little evidence for enhanced phenotypic evolution in
727   early teleosts relative to their living fossil sister group. *Proc. Natl. Acad. Sci.* **113**, 11531–
728   11536. (doi:10.1073/pnas.1607237113)
729   78. Olsen AM, Westneat MW. 2015 StereoMorph: an R package for the collection of 3D
730   landmarks and curves using a stereo camera set-up. *Methods Ecol. Evol.* **6**, 351–356.
731   (doi:10.1111/2041-210X.12326)
732   79. Adams DC, Otárola-Castillo E. 2013 geomorph: an r package for the collection and analysis
733   of geometric morphometric shape data. *Methods Ecol. Evol.* **4**, 393–399. (doi:10.1111/2041-
734   210X.12035)
735   80. Baken EK, Collyer ML, Kaliontzopoulou A, Adams DC. 2021 geomorph v4.0 and gmShiny:
736   Enhanced analytics and a new graphical interface for a comprehensive morphometric
737   experience. *Methods Ecol. Evol.* **12**, 2355–2363. (doi:10.1111/2041-210X.13723)
738   81. Clavel J, Escarguel G, Merceron G. 2015 mvMORPH: an R package for fitting multivariate
739   evolutionary models to morphometric data. *Methods Ecol. Evol.* **6**, 1311–1319.
740   (doi:10.1111/2041-210X.12420)
741   82. Clavel J, Aristide L, Morlon H. 2019 A Penalized Likelihood Framework for High-
742   Dimensional Phylogenetic Comparative Methods and an Application to New-World Monkeys
743   Brain Evolution. *Syst. Biol.* **68**, 93–116. (doi:10.1093/sysbio/syy045)
744   83. Hansen TF. 1997 Stabilizing selection and the comparative analysis of adaptation. *Evolution*
745   **51**, 1341–1351. (doi:10.1111/j.1558-5646.1997.tb01457.x)

746 84. Ho LST, Ané C. 2014 Intrinsic inference difficulties for trait evolution with Ornstein-
747   Uhlenbeck models. *Methods Ecol. Evol.* **5**, 1133–1146. (doi:10.1111/2041-210X.12285)
748 85. Blomberg SP, Garland Jr. T, Ives AR. 2003 Testing for phylogenetic signal in comparative
749   data: behavioral traits are more labile. *Evolution* **57**, 717–745. (doi:10.1111/j.0014-
750   3820.2003.tb00285.x)
751 86. Silvestro D, Kostikova A, Litsios G, Pearman PB, Salamin N. 2015 Measurement errors
752   should always be incorporated in phylogenetic comparative analysis. *Methods Ecol. Evol.* **6**,
753   340–346. (doi:10.1111/2041-210X.12337)
754 87. Konishi S, Kitagawa, Genshiro. 1996 Generalised information criteria in model selection.
755   *Biometrika* **83**, 875–890. (doi:10.1093/biomet/83.4.875)
756 88. Konishi S, Kitagawa G. 2008 *Information Criteria and Statistical Modeling*. New York, NY:
757   Springer New York. (doi:10.1007/978-0-387-71887-3)
758 89. Dollo L. 1895 Sur la phylogénie des Dipneustes. *Bull. Société Belge Géologie Paléontol.*
759   *Hydrol.* **9**, 79–128.
760 90. Ahlberg PE, Trewin NH. 1994 The postcranial skeleton of the Middle Devonian lungfish
761   *Dipterus valenciennesi*. *Trans. R. Soc. Edinb. Earth Sci.* **85**, 159–175.
762   (doi:10.1017/S0263593300003588)
763 91. Friedman M, Daeschler EB. 2006 Late Devonian (Famennian) lungfishes from the Catskill
764   Formation of Pennsylvania, USA. *Palaeontology* **49**, 1167–1183. (doi:10.1111/j.1475-
765   4983.2006.00594.x)
766 92. Hopkins MJ, Lidgard S. 2012 Evolutionary mode routinely varies among morphological traits
767   within fossil species lineages. *Proc. Natl. Acad. Sci.* **109**, 20520–20525.
768   (doi:10.1073/pnas.1209901109)
769 93. Foote M. 1996 Models of morphological diversification. In *Evolutionary Paleobiology* (eds D
770   Jablonski, DH Erwin, JH Lipps), pp. 62–86. Chicago: University of Chicago Press.
771 94. Sidlauskas B. 2008 Continuous and arrested morphological diversification in sister clades of
772   characiform fishes: a phylomorphospace approach. *Evolution* **62**, 3135–3156.
773   (doi:10.1111/j.1558-5646.2008.00519.x)
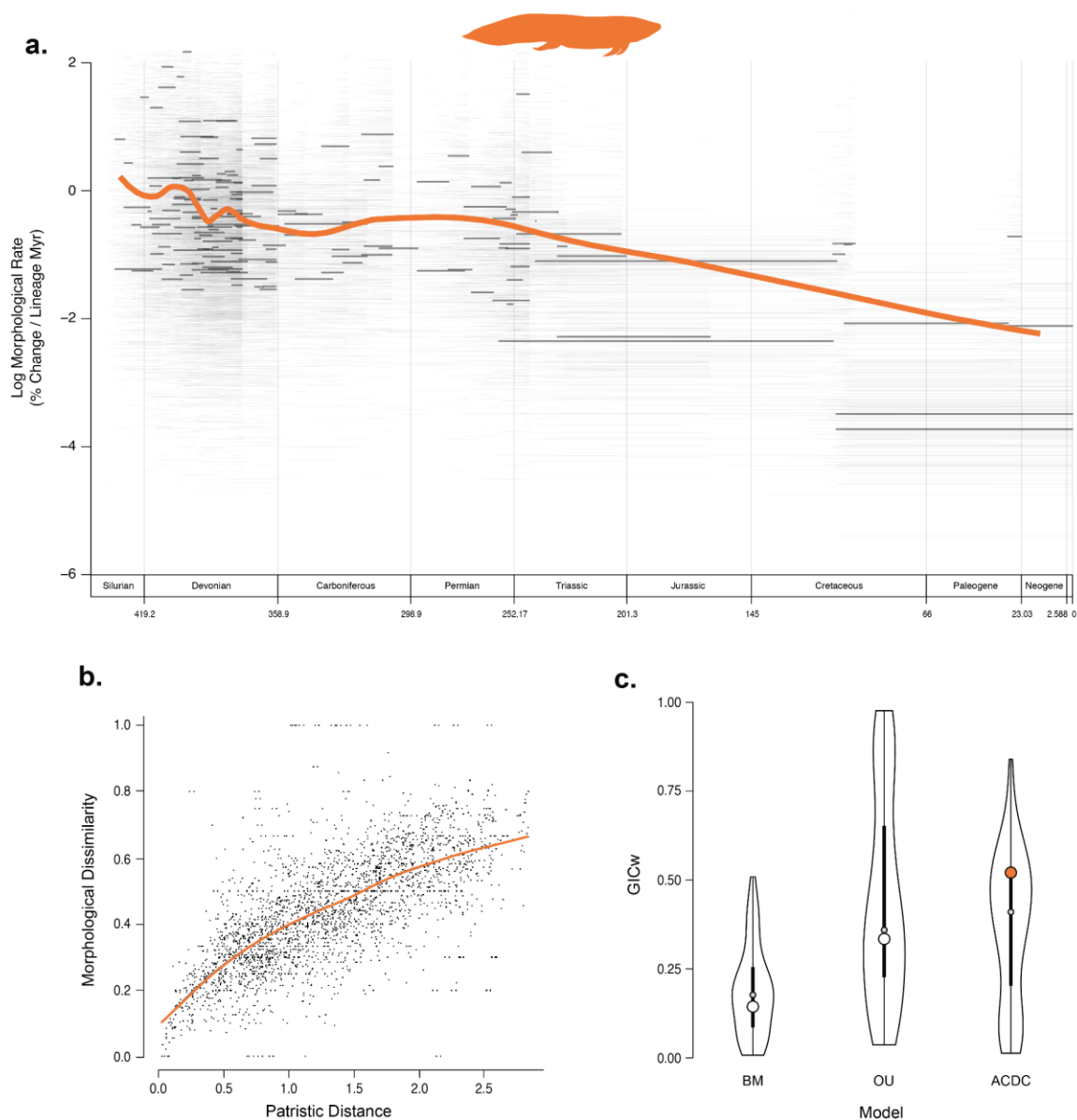774
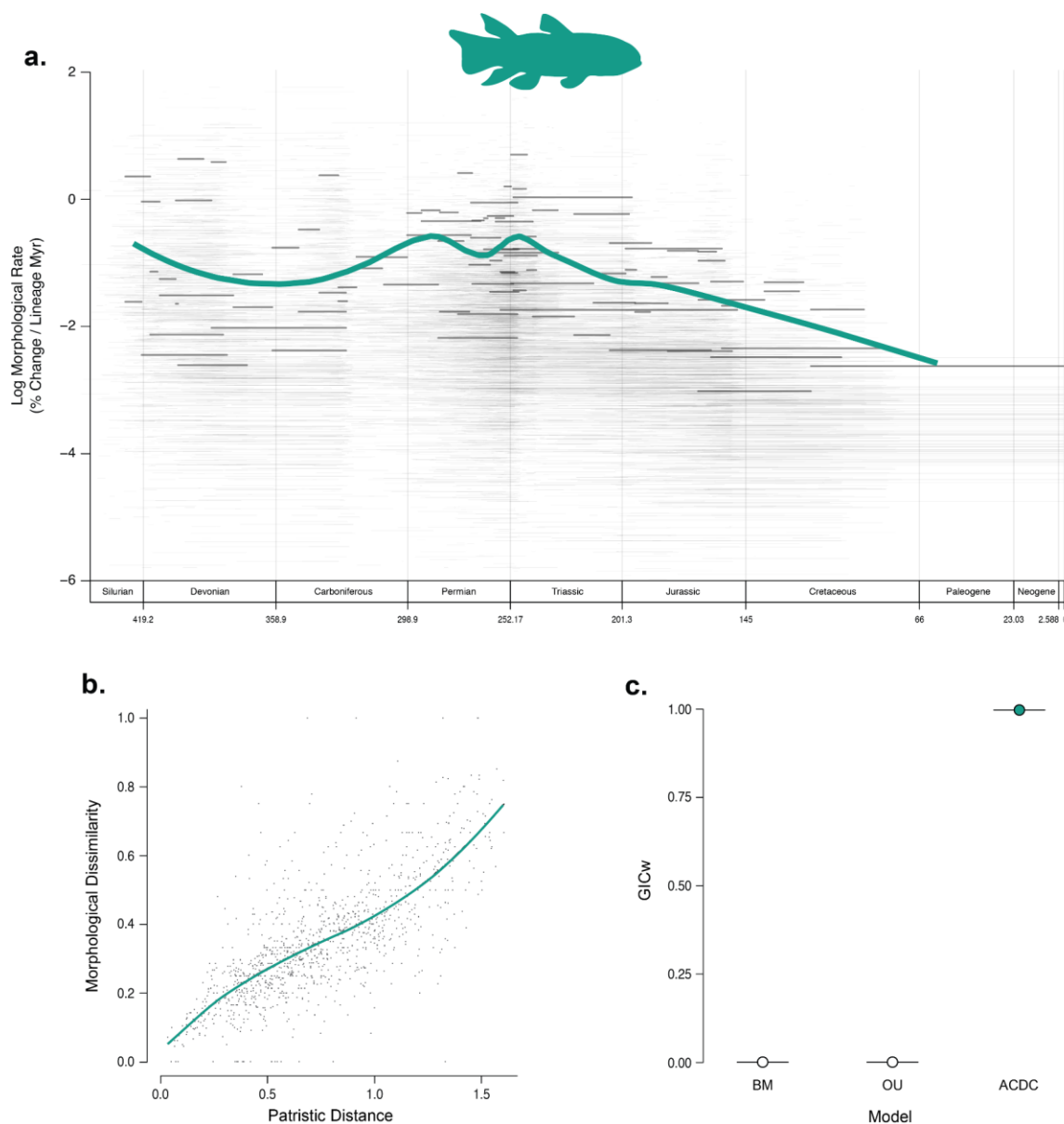
Figures

776

Figure 1. Patterns of phenotypic evolution in coelacanths. (a) rate-through-time plot for discrete

characters, derived from the MCC tree and a random sampling of 100 trees from the posterior

generated using morphological data in BEAST v2.6.5 with the Fossilized Birth-Death model. The

thicker, solid green line is the average rate across the MCC tree; the thinner, solid black lines are
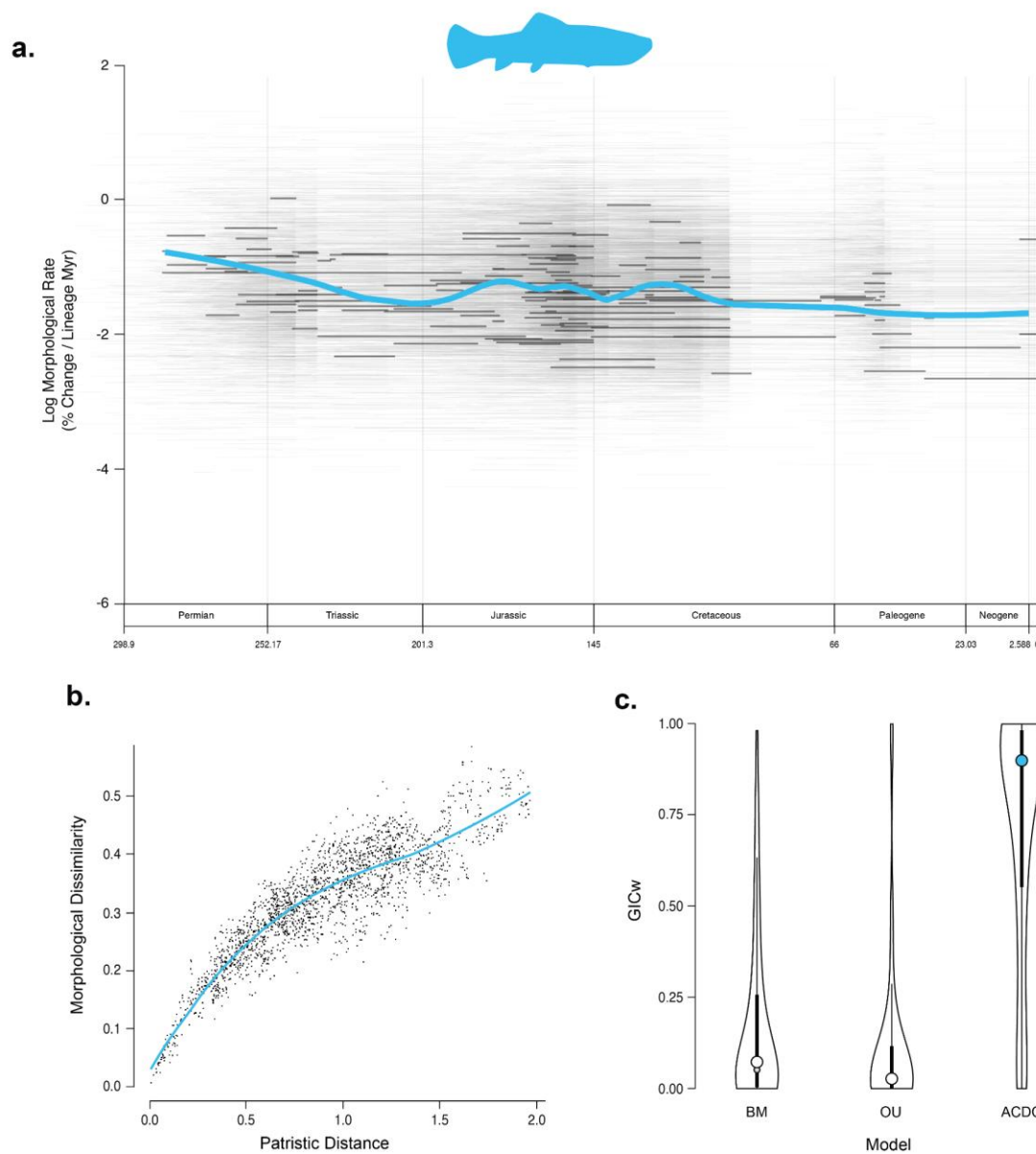
781   the MCC per-branch rates; and the semi-transparent grey lines forming a "cloud" behind the plot

782   are the per-branch rates from each tree sampled from the posterior. Average rate-through-time

783   plots for all groups can be found in Figure S9. (b) character saturation, generated using the discrete

784   character matrix to calculate pairwise character-state dissimilarity and plot it against patristic

785   morphological distance. (c) support for competing models of body-shape evolution (GICw)

786   derived from the MCC tree (larger circles), a sample of 100 posterior trees (violin plot distribution

787   with smaller circles), and the PC axes that summarised 100% of the variability for each clade. The

788   large, coloured circle indicates the highest model support recovered for the MCC tree. The black

789   box plots within the violin plots have smaller, grey circles denoting the median model support

790   across the 100 posterior trees tested. The intervals represented by the boxes and whiskers are the

791   quartiles calculated by the *vioplot* package. Models and *mvMORPH* methods are discussed in the

792   text. Silhouette of *Miguashaia* by Steven Coombs (Public Domain) via PhyloPic.

793

794

Figure 2. Patterns of phenotypic evolution in lungfishes. (a) rate-through-time plot for discrete

characters, derived from the MCC tree and a random sampling of 100 trees from the posterior

generated using morphological data in BEAST v2.6.5 with the Fossilized Birth-Death model. The

thicker, solid orange line is the average rate across the MCC tree; the thinner, solid black lines are

the MCC per-branch rates; and the semi-transparent grey lines forming a "cloud" behind the plot

are the per-branch rates from each tree sampled from the posterior. Average rate-through-time

801   plots for all groups can be found in Figure S9. (b) character saturation, generated using the discrete

802   character matrix to calculate pairwise character-state dissimilarity and plot it against patristic

803   morphological distance. (c) support for competing models of body-shape evolution (GICw)

804   derived from the MCC tree (larger circles), a sample of 100 posterior trees (violin plot distribution

805   with smaller circles), and the PC axes that summarised 100% of the variability for each clade. The

806   large, coloured circle indicates the highest model support recovered for the MCC tree. The black

807   box plots within the violin plots have smaller, grey circles denoting the median model support

808   across the 100 posterior trees tested. The intervals represented by the boxes and whiskers are the

809   quartiles calculated by the *vioplot* package. Models and *mvMORPH* methods are discussed in the

810   text. Silhouette of *Ceratodus* by T. Michael Keesey (Public Domain) via PhyloPic.

811

Figure 3. Patterns of phenotypic evolution in holosteans. (a) rate-through-time plot for discrete characters, derived from the MCC tree and a random sampling of 100 trees from the posterior generated using morphological data in BEAST v2.6.5 with the Fossilized Birth-Death model. The thicker, solid blue line is the average rate across the MCC tree; the thinner, solid black lines are the MCC per-branch rates; and the semi-transparent grey lines forming a "cloud" behind the plot are the per-branch rates from each tree sampled from the posterior. Average rate-through-time

819   plots for all groups can be found in Figure S9. (b) character saturation, generated using the discrete

820   character matrix to calculate pairwise character-state dissimilarity and plot it against patristic

821   morphological distance. (c) support for competing models of body-shape evolution (GICw)

822   derived from the MCC tree (larger circles), a sample of 100 posterior trees (violin plot distribution

823   with smaller circles), and the PC axes that summarised 100% of the variability for each clade. The

824   large, coloured circle indicates the highest model support recovered for the MCC tree. The black

825   box plots within the violin plots have smaller, grey circles denoting the median model support

826   across the 100 posterior trees tested. The intervals represented by the boxes and whiskers are the

827   quartiles calculated by the *vioplot* package. Models and *mvMORPH* methods are discussed in the

828   text. Silhouette of *Calamopleurus* by Aline M. Ghilardi (CC BY-NC 3.0) via PhyloPic.